

An extended cloud analysis method for seismic fragility assessment of highway bridges

Mohammad Ghalami Sfahani^{*} and Hong Guan^a

Griffith School of Engineering and Built Environment, Griffith University Gold Coast Campus, Queensland 4222, Australia

(Received June 6, 2018, Revised September 29, 2018, Accepted October 24, 2018)

Abstract. In this paper, an extended Cloud analysis method is developed for seismic fragility assessment of existing highway bridges in the southeast Queensland region. This method extends the original Cloud analysis dataset by performing scaled Cloud analyses. The original and scaled Cloud datasets are then paired to generate seismic fragility curves. The seismic hazard in this region is critically reviewed, and the ground motion records are selected for the time-history analysis based on various record selection criteria. A parametric highway bridge model is developed in the OpenSees analysis software, and a sampling technique is employed to quantify the uncertainties of highway bridges ubiquitous in this region. Technical recommendations are also given for the seismic performance evaluation of highway bridges in such low-to-moderate seismic zones. Finally, a probabilistic fragility study is conducted by performing a total of 8000 time-history analyses and representative bridge fragility curves are generated. It is illustrated that the seismic fragility curves generated by the proposed extended Cloud analysis method are in close agreement with those which are obtained by the rigorous incremental dynamic analysis method. Also, it reveals that more than 50% of highway bridges existing in southeast Queensland will be damaged subject to a peak ground acceleration of 0.14 g.

Keywords: fragility curve; highway bridge; Southeast Queensland; seismic hazard; ground motion record; bridge performance level; time-history analysis; failure probability

1. Introduction

A fundamental task in structural safety evaluation is the seismic fragility assessment, which gives a significant tool for long-term seismic performance prediction of structures. In this regard, extensive studies have been carried out pertaining to different fragility assessment methods (Fajfar 2000, Cornell *et al.* 2002, Vamvatsikos and Cornell 2002, Jalayer 2003, Baker 2015) and bridge structures (Choi *et al.* 2004, Nielson and DesRoches 2007, Aviram *et al.* 2008, Padgett and DesRoches 2008, Franchin and Pinto 2009, Cardone *et al.* 2011, Kaviani *et al.* 2012, Olmos *et al.* 2012, Ebrahimian *et al.* 2015, Akhoondzade-Noghabi and Bargi 2016). The analytical bridge fragility curves are generated based on the analysis of numerical bridge models subjected to simulated seismic loads. A seismic fragility curve depicts the failure probability, P , with respect to a structural performance level at increasing intensity measures (IM) of ground motions (Cornell and Krawinkler 2000, Cornell *et al.* 2002, Ghalami Sfahani *et al.* 2015). The performance levels are represented by numerical limit-state (LS) values in the fragility function, in terms of an engineering demand parameter (EDP). The fragility curves are principally generated for the as-built condition of bridges (Choi *et al.* 2004, Nielson and DesRoches 2007, Cardone *et al.* 2011, Kaviani *et al.* 2012) but can be updated according to the

aging conditions of bridges (Ebrahimian *et al.* 2015) and/or damaged condition of bridges (Franchin and Pinto 2009, Ebrahimian *et al.* 2014). Using the analytical fragility curves, quantitative seismic risk exposure data can be presented to the bridge decision-makers to assist them in recommending an appropriate rehabilitation level based on their engineering judgements. For example, a retrofit prioritisation scheme can be utilised which permits identification of the most susceptible bridges in a road network, the most vulnerable components of those identified bridges and the impact of different retrofit strategies on the performance enhancement of those bridges and their network (Padgett and DesRoches 2008).

Different analytical methods can be adopted for seismic fragility assessment such as the capacity spectrum method (CSM) (Fajfar 2000), multiple stripe analysis (MSA) (Baker 2015), incremental dynamic analysis (IDA) (Vamvatsikos and Cornell 2002) and Cloud analysis methods (Jalayer 2003). The performances of these methods are different in terms of their integrity of simulation, efficiency of computation and versatility in application. For example, those based on the time-history analysis (THA) (e.g., MSA, IDA and Cloud analysis) are widely recognised for the higher degree of integrity they exhibit in simulating seismic loads. Also, the Cloud analysis is recognised for being the most efficient THA-based method, as it requires as few as one THA for each ground motion record (GMR) used for the analysis. However, some inherent limitations of the original Cloud analysis (OCA) method make its application less versatile in wide ranges of IMs, in comparison with IDA and MSA. To be specific, in the absence of scaled derivatives of the utilised GMRs for the THA, the seismic

*Corresponding author, Associate Lecturer
E-mail: m.ghalamisfahani@griffith.edu.au

^aProfessor

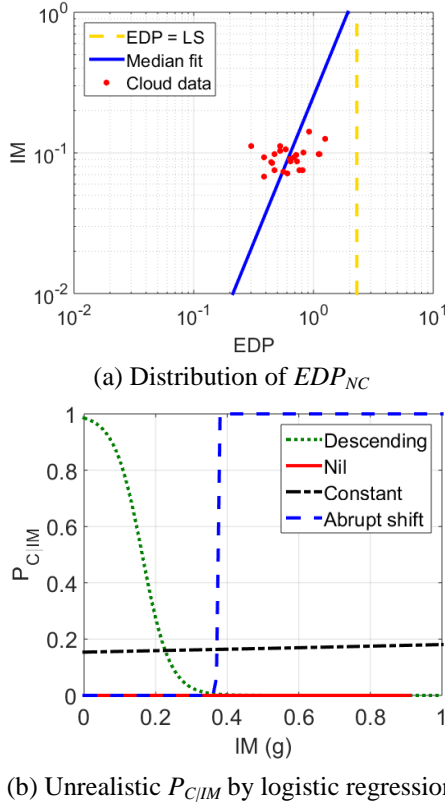


Fig. 1 Common issues with the original Cloud analysis method

fragility results become highly susceptible to the selected records. In particular, the non-collapse EDPs (i.e., EDP_{NC}) which are distributed within a narrow range of structural ductility are considered to be inadequate and therefore inaccurate in representing the actual structural behaviour. Fig. 1(a) illustrates an example of such an inadequate distribution where all the estimated EDPs by the OCA (red dot-points) are less than the LS line (yellow dash line). Such observation impacts the trend of the fitted median line (i.e., the blue solid line), and thereby the fragility curve, since the behaviour of the bridge with high nonlinearity is not captured. In addition, using the OCA data the collapse seismic fragility assessment is only possible through performing the logistic regression, which is highly sensitive to the distribution of collapse IMs (IM_C) with respect to the non-collapse IMs (IM_{NC}). Fig. 1(b) shows four probable cases where the resultant logistic regression can become unstable, as it brings about unrealistic envelopes of the collapse probability ($P_{C/IM}$) over the range of IMs. These are estimating $P_{C/IM}$ as nil (solid red line) or a constant value (black dash-dot line) over the entire range of IMs, a descending trend for the $P_{C/IM}$ with increasing IMs (green dotted line), and an abrupt shift from $P_{C/IM}=0$ to $P_{C/IM}=1$ in a very narrow range of IM (blue dash line).

It should be noted that the currently available GMR selection techniques in the literature (Baker 2010, Jayaram *et al.* 2011) have principally been developed in compliance with the rigorous THA-based seismic fragility assessment methods (e.g., IDA and MSA). With respect to GMR selection for the OCA, using the conventional filtering

method also would not guarantee elimination of the abovementioned limitations while this method can also yield biased analysis results. In this paper, to overcome the limitations of the OCA, an improved method called the extended Cloud analysis (ECA) is proposed. The ECA method extends the OCA data by performing scaled Cloud analyses (SCA) and then pairs the two analysis (i.e., OCA and SCA) datasets for seismic fragility assessment. Although this inevitably lowers the computational efficiency by using the ECA method, the enhanced versatility for seismic fragility assessment motivates the use of this method. For this purpose, a stepwise process for performing the seismic fragility assessment using the ECA method is described in Section 2, which is implemented by the GMRs selected in Section 3 and the bridge models developed in Section 4. Finally, relevant illustrations of the seismic fragility results and detailed discussion are presented in Section 5.

2. Extended cloud analysis

The step-by-step procedure to perform analytical seismic fragility assessment of structures using the proposed ECA method is illustrated in the flowchart shown in Fig. 2.

- Steps 1 and 2: These steps contribute to the GMR selection and the finite element (FE) modelling for the THA, respectively, which are discussed in the subsequent sections.
- Step 3: The OCA is performed to evaluate the linear median fit to the $IM_{NC}-EDP_{NC}$ data in the sampling logarithmic space (e.g., see Fig. 1(a)).
- Step 4: The selected GMRs in the first step are scaled and utilised for performing the SCA, on the FE models developed in the second step.

Different scaling approaches have been proposed and examined for this purpose and a “*transition*” scaling approach was found to be more suitable for this task (Ghalami Sfahani 2017). This approach shifts the non-collapse OCA data toward a LS value corresponding to the targeted structural performance level for seismic fragility assessment. To achieve this, the following scale factor is proposed to match the medians of the non-collapse EDPs and IMs of the OCA data to the targeted structural performance level in the sampling logarithmic space. Or

$$SF_{transition} = \sqrt{\left(\frac{LS}{\eta_{EDP}}\right)^2 + \left(\frac{IM_{LS}}{\eta_{IM}}\right)^2} \quad (1)$$

where LS is the limit-state corresponding to the targeted structural performance level, η_{EDP} is the median of the EDP_{NC} estimated by OCA, IM_{LS} is the IM level at which the median fit and the $EDP = LS$ lines intersect in the sampling logarithmic space, and η_{IM} is the median of the original IM_{NC} levels. Note that the SCA data obtained by the “*transition*” scaling approach can be utilised independently to perform seismic fragility assessment based on the Cloud analysis method.

- Step 5: The IM-EDP data estimated by the OCA and SCA are paired for each GMR.

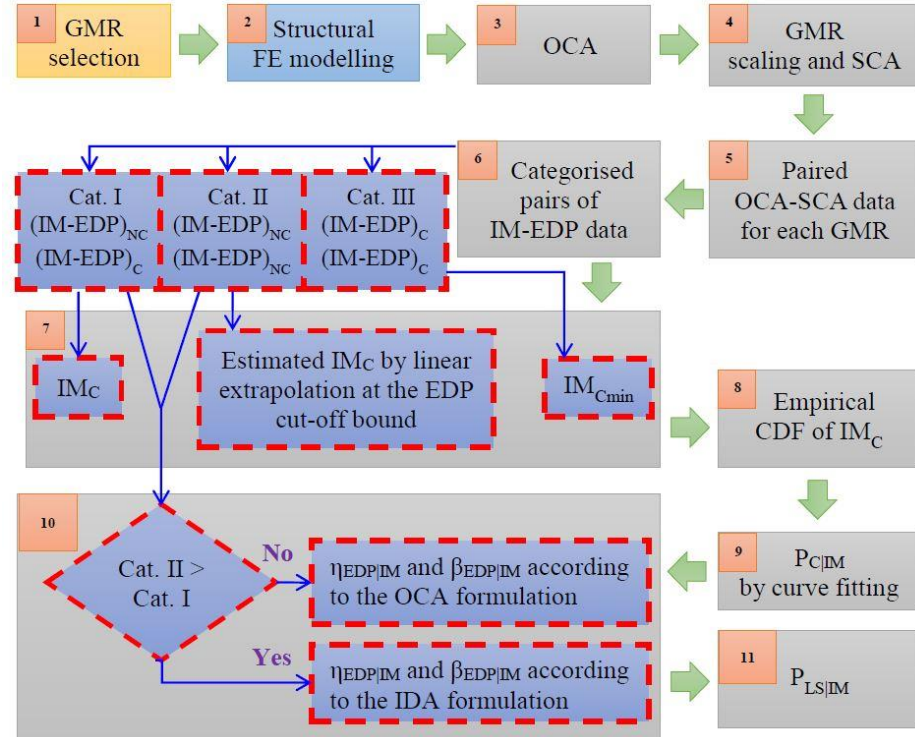


Fig. 2 Seismic fragility assessment based on the ECA method

- Step 6: The pairs of IM-EDP data are divided into three different categories.

These categories are Cat. I containing a non-collapse case ($IM-EDP$)_{NC} paired with a collapse case ($IM-EDP$)_C; Cat. II containing pairs of two non-collapse cases ($IM-EDP$)_{NC}; and Cat. III containing pairs of two collapse cases ($IM-EDP$)_C.

- Step 7: The IM_C level is identified for all the GMRs in use.

The IM_C values are sampled from Cat. I and then the minimum IM_C values, IM_{Cmin} , are sampled from Cat. III. For the GMRs in Cat. II, a linear extrapolation is recommended to estimate IM_C at the EDP cut-off bounds, as the collapse criteria considered in THA, using the pairs of $IM_{NC}-EDP_{NC}$ data in the logarithmic space.

- Step 8: The IM_C levels identified for different GMRs are sorted ascendingly to develop an empirical cumulative density function (CDF).

- Step 9: A curve is fitted to the CDF of IM_C levels, using the maximum likelihood method (Baker 2015), which depicts the $P_{C|IM}$ based on the ECA method.

- Step 10: The median fit ($\eta_{EDP|IM}$) and the standard deviation ($\beta_{EDP|IM}$) of distribution of non-collapse analysis data are evaluated using either Cat. I or Cat. II.

Depending on the higher number of GMRs. If Cat. I data is utilised the OCA formulation (Jalayer 2003, Ghalami Sfahani 2017) must be used for $\eta_{EDP|IM}$ and $\beta_{EDP|IM}$. Otherwise, the IDA formulation (Jalayer 2003, Ghalami Sfahani 2017) is recommended to be utilised for $\eta_{EDP|IM}$ and $\beta_{EDP|IM}$ using the Cat. II analysis data.

- Step 11: The seismic fragility ($P_{LS|IM}$) with respect to a performance level (i.e., numerically represented by a LS value) is obtained at increasing IMs as follows

$$P_{LS|IM=x} = \Phi \left(\frac{\log LS - \log \eta_{EDP|IM=x}}{\beta_{EDP|IM=x}} \right) \quad (2)$$

where Φ is the standardised Gaussian (normal) CDF (Benjamin and Cornell 1970).

3. Seismic hazard and ground motion records

As demonstrated in Fig. 2, Step 1 of the ECA process contributes to the selection of GMRs. In this study, the southeast Queensland region of Australia is considered as the site of interest for being the most populated area and the economic and cultural region of the state. Fig. 3 shows the seismic hazard map of this region in a 2500-year return period and in terms of the peak ground acceleration (PGA) (Leonard, Burbidge *et al.* 2013). As seen, it seems that the highest possible shaking in southeast Queensland would be less than PGA=0.2 g, which classifies this region as a low-to-moderate seismic zone. However, it should be noted that such maps are developed based on the probabilistic seismic hazard analysis (PSHA) (Cornell 1968, Leonard *et al.* 2014) and can largely be uncertain for Australia since they could barely be validated by strong onshore earthquakes (Leonard *et al.* 2013, Leonard *et al.* 2014).

One major difficulty associated with GMR selection is that highway bridges are sparse in the southeast Queensland road network and they are constructed on various geotechnical conditions. Hence, selection of all GMRs based on a specific criterion will misrepresent the seismicity of southeast Queensland. As such, four suites of GMRs are selected based on different selection methods and criteria,

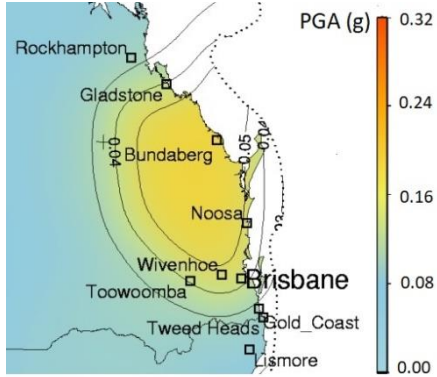
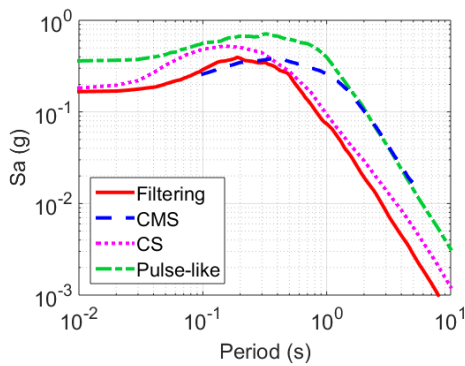
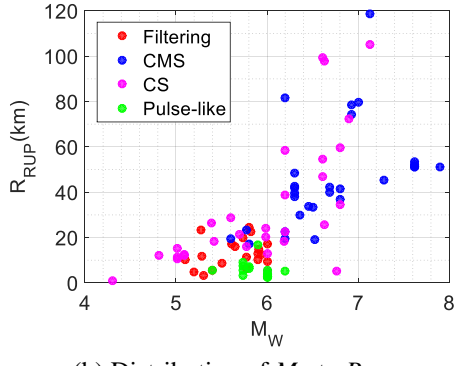


Fig. 3 2500-year return period seismic hazard map of southeast Queensland



(a) Acceleration response spectra



(b) Distribution of M_W to R_{RUP}

Fig. 4 Characteristics of selected ground motion records

from the PEER NGA-West2 database (Ancheta *et al.* 2014). These include 20 GMRs selected by the conventional filtering method as suite #1, 30 GMRs by the conditional mean spectrum (CMS) method (Baker 2010) as suite #2, 30 GMRs by the conditional spectrum method (Jayaram *et al.* 2011) as suite #3, and 20 pulse-like GMRs as suite #4. This make a total of 100 GMRs. The name of the seismic event, the year of occurrence and the record sequence number (RSN) of these GMRs are summarised in Table 1. Fig. 4(a) illustrates the mean acceleration response spectra of these GMR suites. The target mean response spectrum for GMR selection by the CMS method was a 2% in 50-year uniform hazard spectrum of Ee subsoil site condition in southeast Queensland (AS1170.4 2007). For the conditional spectrum method, the target mean and variance spectra were evaluated by a ground motion prediction equation proposed

Table 1 Selected suites of ground motion records

RSN*	Event name	Year	RSN	Event name	Year
GMR suite #1					GMR suite #3
96	"Managua_Nicaragua-02"	1972	34	"Northern Calif-05"	1967
132	"Friuli_Italy-02"	1976	199	"Imperial Valley-07"	1979
134	"Izmir_Turkey"	1977	203	"Imperial Valley-07"	1979
154	"Coyote Lake"	1979	208	"Imperial Valley-07"	1979
248	"Mammoth Lakes-06"	1980	223	"Livermore-02"	1980
405	"Coalinga-05"	1983	383	"Coalinga-02"	1983
445	"New Zealand-01"	1984	385	"Coalinga-02"	1983
485	"Bishop (Rnd Val)"	1984	411	"Coalinga-05"	1983
547	"Chalfant Valley-01"	1986	497	"Nahanni_Canada"	1985
565	"Kalamata_Greece-02"	1986	550	"Chalfant Valley-02"	1986
1099	"Double Springs"	1994	600	"Whittier Narrows-01"	1987
1135	"Kozani_Greece-04"	1995	668	"Whittier Narrows-01"	1987
1646	"Sierra Madre"	1991	1623	"Stone Canyon"	1972
1725	"Northridge-06"	1994	1825	"Hector Mine"	1999
1740	"Little Skull Mtn_NV"	1992	2623	"Chi-Chi_Taiwan-03"	1999
2391	"Chi-Chi_Taiwan-02"	1999	3186	"Chi-Chi_Taiwan-05"	1999
3605	"Lazio_Abruzzo_Italy"	1984	3217	"Chi-Chi_Taiwan-05"	1999
3699	"Whittier Narrows-02"	1987	3905	"Tottori_Japan"	2000
4147	"Parkfield-02_CA"	2004	3923	"Tottori_Japan"	2000
4348	"Umbria Marche_Italy"	1997	4083	"Parkfield-02_CA"	2004
GMR suite #2					4085 "Parkfield-02_CA" 2004
26	"Hollister-01"	1961	4177	"Niigata_Japan"	2004
122	"Friuli_Italy-01"	1976	4213	"Niigata_Japan"	2004
214	"Livermore-01"	1980	4336	"Umbria Marche_Italy"	1997
302	"Irpinia_Italy-02"	1980	4395	"Umbria Marche_Italy"	1997
346	"Coalinga-01"	1983	4870	"Chuetsu-oki_Japan"	2007
544	"Chalfant Valley-01"	1986	5292	"Chuetsu-oki_Japan"	2007
793	"Loma Prieta"	1989	5649	"Iwate_Japan"	2008
797	"Loma Prieta"	1989	6239	"Tottori_Japan"	2000
930	"Big Bear-01"	1992	8771	"14383980"	2008
981	"Northridge-01"	1994		GMR suite #4	
1026	"Northridge-01"	1994	147	"Coyote Lake"	1979
1266	"Chi-Chi_Taiwan"	1999	148	"Coyote Lake"	1979
1267	"Chi-Chi_Taiwan"	1999	149	"Coyote Lake"	1979
1268	"Chi-Chi_Taiwan"	1999	150	"Coyote Lake"	1979
1280	"Chi-Chi_Taiwan"	1999	316	"Westmorland"	1981
1296	"Chi-Chi_Taiwan"	1999	566	"Kalamata_Greece-02"	1986
1784	"Hector Mine"	1999	568	"San Salvador"	1986
2107	"Denali_Alaska"	2002	569	"San Salvador"	1986
2626	"Chi-Chi_Taiwan-03"	1999	4065	"Parkfield-02_CA"	2004
2937	"Chi-Chi_Taiwan-05"	1999	4097	"Parkfield-02_CA"	2004
3465	"Chi-Chi_Taiwan-06"	1999	4098	"Parkfield-02_CA"	2004
3494	"Chi-Chi_Taiwan-06"	1999	4100	"Parkfield-02_CA"	2004

Table 1 Continued

3495	"Chi-Chi_Taiwan-06"	1999	4101	"Parkfield-02_CA"	2004
3504	"Chi-Chi_Taiwan-06"	1999	4102	"Parkfield-02_CA"	2004
3752	"Landers"	1992	4103	"Parkfield-02_CA"	2004
3867	"Chi-Chi_Taiwan-06"	1999	4107	"Parkfield-02_CA"	2004
4013	"San Simeon_CA"	2003	4113	"Parkfield-02_CA"	2004
4851	"Chuetsu-oki_Japan"	2007	4115	"Parkfield-02_CA"	2004
5268	"Chuetsu-oki_Japan"	2007	4126	"Parkfield-02_CA"	2004
6992	"Darfield_New Zealand"	2010	8123	"Christchurch_NZ"	2011

*RSN: Record Sequence Number

for an Australian earthquake (Somerville, Graves *et al.* 2009) with magnitude of $M_W=6.0$ and rupture distance $R_{RUP}=10$ km at a rock site condition. These target spectra are more than 98% matched with the mean spectra illustrated in Fig. 4(a). Also, Fig. 4(b) shows the M_W - R_{RUP} distribution for the selected earthquake records. As seen, a low magnitude (i.e., $M_W \leq 6.0$) near-to-source (i.e., $R_{RUP} < 25$ km) earthquake scenario was considered for selecting the GMRs in the filtering and pulse-like suites.

4. Highway bridge structures

A multi-span concrete overpass is a common class of highway bridges in Australia's road network, due to their

cost-efficiency and simplicity of the design and construction. These bridges are generally constructed with various configurations of prefabricated decks supported on reinforced concrete (RC) piers in the middle of the bridge, and RC abutments at the bridge ends (Nielson and DesRoches 2007, Ghalami Sfahani *et al.* 2015). In this study, a three-dimensional numerical model of this type of bridges is developed to investigate their seismic performances.

4.1 Structural modelling

As discussed previously, Step 2 for performing ECA involves creating a structural FE model. In this study, a parametric FE model is created for highway bridges in the OpenSees analysis software (McKenna *et al.* 2015). Fig. 5 illustrates this bridge model. The model for the superstructure deck is comprised of an elastic beam in the bridge longitudinal direction which is attached to perpendicular rigid beams at deck ends to simulate the transverse behaviour. Adequate number of nodes are assigned along each of these beams to simulate lump mass along the elastic beam and define deck's bearings and expansion joints along the rigid beams. Also, the bridge piers can be simulated by a layered shell model (Lu *et al.* 2015) and/or a fibre beam model (Scott and Fenves 2006) in OpenSees, depending on their configuration. The dynamic responses of other bridge components are simulated analytically by zero-length springs in OpenSees. These springs include a bilinear hardening spring for the expansion joints (Muthukumar and DesRoches 2006), an elastic-perfectly-plastic spring for the abutment's

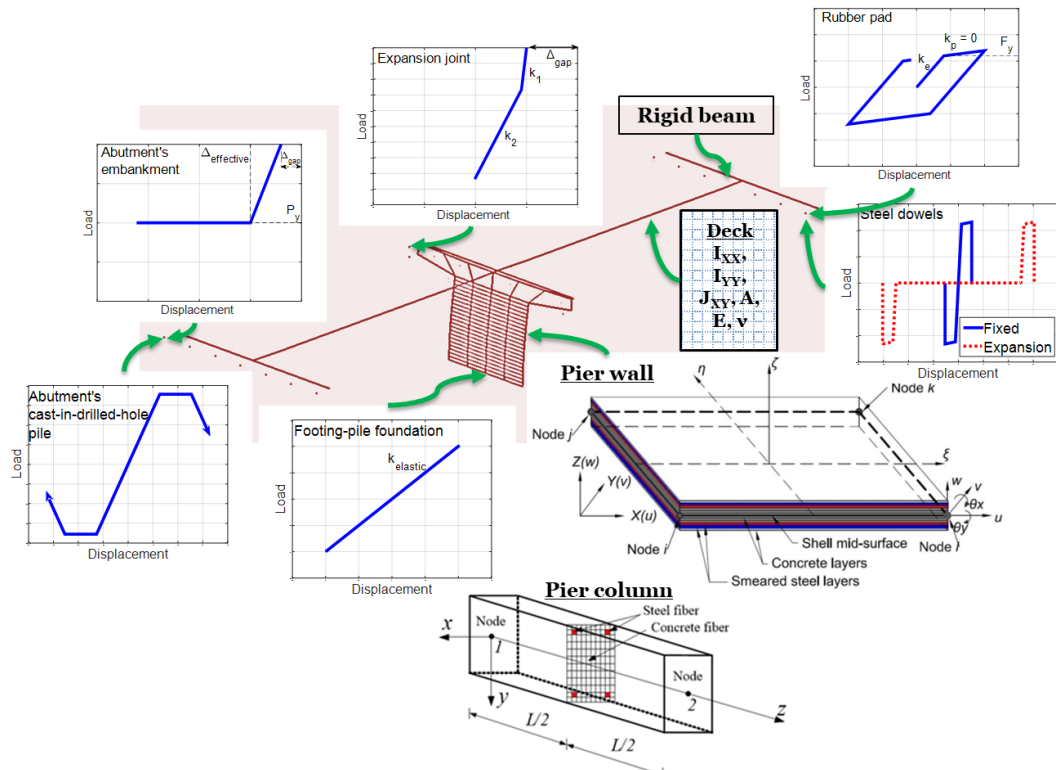


Fig. 5 Structural FE model of highway bridges in OpenSees

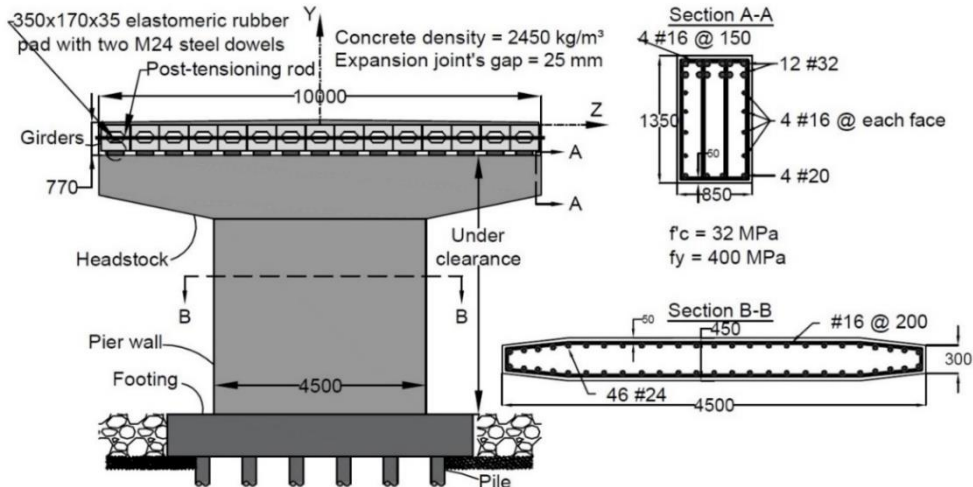


Fig. 6 Details of bridge piers

embankment in the longitudinal passive direction (Aviram *et al.* 2008), a degrading hysteretic spring for the abutment's pile (Caltrans 2013), and a linear elastic spring for the pier's footing (DesRoches *et al.* 2003). In addition, the simply supported bearing system of highway bridge decks is often provided by a combination of elastomeric rubber pads and steel dowels. The dynamic responses of this bearing system are simulated by an elastic-perfectly-plastic spring for the pad in parallel with a degrading hysteretic spring for the dowels (Choi *et al.* 2004).

The configuration, dimensions and material properties of a typical bridge pier are illustrated in Fig. 6. These are taken from an existing highway bridge in the southeast Queensland which has been designed and constructed before 2004, i.e., prior to (AS5100.2 2004), without incorporating any seismic provision. To enhance the reliability of fragility assessment for the southeast Queensland highway bridges the uncertainties in the developed bridge models are accounted for by using eight uncertain modelling parameters from the sampling process. These parameters are the concrete compressive strength (f'_c), steel yielding strength (f_y), deck mass (%), damping ratio (%), number of abutment piles, number of spans, span length (m), and height of under-clearance (m). The Latin Hypercube sampling (LHS) technique (Ayyub and Lai 1989) is utilised for this sampling task. Table 2 summarises a total of forty sampled bridge models which are generated for seismic fragility assessment of highway bridges in the southeast Queensland region. Each model is paired with the one hundred GMRS selected in Section 3. Subsequently, 8000 THA are performed at the original and scaled IM levels of selected GMRS, based on the ECA method.

4.2 Seismic performance

One significant task for seismic fragility assessment of structures is to characterise the targeted structural performance levels qualitatively and nominating numerical representative LSs of each performance level quantitatively. In this study, three performance levels are recommended for the highway bridges in Australia, namely the operational

Table 2 Sampled highway bridge models for southeast Queensland

Sampled bridge model	Uncertain bridge modelling parameters							
	f'_c MPa	f_y MPa	Deck mass (%)	Damping ratio (%)	Number of piles	Span length (m)	Under-clearance (m)	
1	36.21	501.36	91.75	6.42	4	6	14.4	5.4
2	28.58	449.05	109.75	3.98	3	5	17.1	6.3
3	40.40	421.02	90.25	3.89	3	2	20.8	4.9
4	39.63	424.65	103.75	6.02	7	7	15.6	5.2
5	43.44	519.43	100.25	4.86	6	5	17.4	6.1
6	34.20	465.25	93.25	2.98	5	7	22.3	6.6
7	32.29	486.46	93.75	4.46	7	8	9.2	6.5
8	31.39	472.55	100.75	3.71	5	4	9.6	7.3
9	32.00	416.94	107.75	4.22	9	8	17.8	8.0
10	29.99	453.69	101.25	2.58	6	3	18.6	5.8
11	29.57	436.66	101.75	3.14	9	5	20.1	8.2
12	30.73	493.23	97.75	5.29	2	6	8.1	6.4
13	36.53	446.69	90.75	4.14	8	6	21.2	5.7
14	31.07	506.27	106.25	4.38	2	9	16.3	5.6
15	30.37	406.37	108.25	4.78	3	6	9.9	8.7
16	31.70	462.91	92.25	4.30	9	4	11.8	7.5
17	38.03	470.06	105.25	4.54	3	9	16.7	8.4
18	29.11	444.28	99.75	4.62	7	7	18.9	6.2
19	39.02	427.96	96.75	6.20	8	6	15.9	7.8
20	36.87	512.09	109.25	5.11	3	5	14.1	5.9
21	33.40	384.02	106.75	7.30	4	5	12.6	7.2
22	38.49	497.07	97.25	3.27	5	4	13.3	7.1
23	34.75	549.67	92.75	5.50	7	3	20.4	6.9
24	32.85	398.44	94.75	5.39	5	8	14.8	7.7
25	33.93	431.03	95.75	4.94	5	2	21.9	7.4
26	35.60	477.76	95.25	2.27	2	4	8.8	7.6
27	27.97	529.77	98.25	3.80	4	2	19.7	6.7
28	35.31	451.38	108.75	5.86	8	8	7.7	7.9
29	35.90	489.71	1102.25	3.39	6	4	21.6	7.0
30	35.03	458.29	98.75	4.70	4	7	8.4	5.3
31	37.61	475.11	102.75	3.50	6	8	10.3	5.1
32	24.16	412.19	104.75	5.73	8	6	18.2	8.5
33	27.20	480.51	94.25	2.80	5	8	10.7	5.0
34	33.12	467.64	96.25	5.61	8	9	12.9	8.6
35	37.23	455.99	99.25	5.02	7	3	15.2	6.8
36	26.14	433.92	107.25	4.06	6	3	19.3	8.3
37	34.48	441.82	91.25	5.20	6	3	11.4	6.0
38	33.67	483.40	103.25	6.73	8	5	12.2	5.5
39	41.46	439.28	105.75	3.61	3	7	13.7	6.8
40	32.57	460.59	104.25	1.70	4	3	11.1	8.1

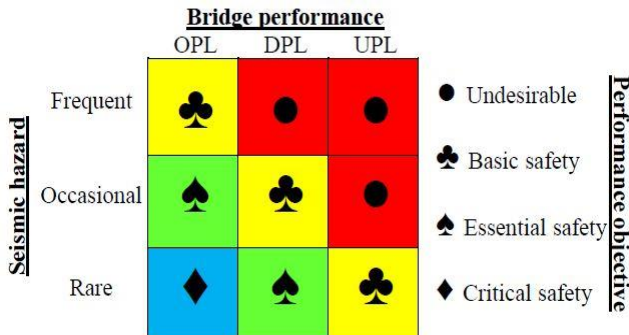


Fig. 7 Desired bridge performance objectives in relation to seismic hazard levels

(OPL), damaged (DPL) and unstable (UPL) performance levels. These bridge performance levels are recommended analogous to the PEER performance-based earthquake engineering methodology (Günay and Mosalam 2013), in relation to the 50% (frequent seismic event), 10% (occasional seismic event) and 2% (rare seismic event) probability of occurrence in a 50-year return period seismic hazard levels, correspondingly. The relationships between the seismic hazard levels, bridge performance levels and the targeted performance objectives are depicted in Fig. 7. Detailed explanations of recommended bridge performance levels are summarised in Table 3. For each level, the estimated consequences of damage and the bridge component and material behaviour are explained, and representative LSs are given.

To link the described bridge performance levels, in Table 3, to the FE models utilised for the highway bridge components in this study, the dynamic behaviour and seismic responses of these models are illustrated in Fig. 8. The nonlinear static pushover analysis is performed in the out-of-plane (Fig. 8(a)) and in-plane directions (Fig. 8(b)) of the bridge pier wall. The onsets of yield (i.e., yielding of the most outer longitudinal reinforcing bars), peak (i.e., maximum base shear capacity), and ultimate (i.e., 20% drop in the base shear capacity) capacity points are also marked on these pushover curves. The dynamic response of the bearing system consisting of elastomeric rubber pad and steel dowels is demonstrated in Fig. 8(c). For the fixed-type bearings, this response is identical in the bridge longitudinal and transverse directions. The dynamic response of the expansion-type bearings is also similar to the fixed-type one, however, the hysteretic behaviour of the steel dowels (i.e., the pulse-like load cycles) appears later due to the presence of expansion joint gaps. The expansion joints only exhibit severe hardening behaviour when the expansion gaps between two adjacent decks or decks and abutments are closed (see Fig. 8(d)). The load-displacement behaviour of the model utilised for bridge abutment-pile system is illustrated in Figs. 8(e)-(f). This behaviour is similar in the longitudinal and transverse directions. However, the initial stiffness of the abutment in the longitudinal-passive direction (i.e., negative direction; see Fig. 8(f)) is larger than that in the other directions, due to the passive resistance of the abutment back wall.

Table 3 Descriptions of recommended bridge performance levels

Operational performance level, OPL	Damaged performance level, DPL	Unstable performance level, UPL
General explanations and estimated consequences		
Slight structural damage; minor or no structural repair; no traffic interruption; road networks remain functional	Moderate to extensive structural damage; bridge rehabilitation is necessary; temporary road closure and detours are required	Total loss of the bridge lateral resistance; slight margin to absolute collapse; substantial rehabilitation; long blockage of road networks
Bridge component and material behaviour		
Linear behaviour in properties; some concrete cracking but elastic stress-strain response of reinforcing steel; linear contact between structural assemblies	Notable residual deformation in shear and flexural cracking leading to significant plastic rotation of piers; initial lateral spreading and failure of shear keys in abutments	Initial de-bonding between decks and piers and/or abutments; reinforcement bar slipping and piers' initial buckling; shear failure of RC piers; rotation and settlement of abutments
Representative LS and seismic capacity		
Maximum friction force and/or yield deformation in bearings; yield strain in bridge piers' longitudinal reinforcement; closure of expansion joint gaps; piles yield deformation	Displacement capacity of bearings; piers' 50% ultimate flexural ductility; active displacement resistance (pull) of abutments; ultimate deformation capacity of shear keys	Initial unseating of bridge decks; flexural ductility corresponding to peak resisting shear force; shear resistance of RC piers; passive displacement (push) resistance of abutments

Table 4 Median LS at different performance levels and collapse criteria for highway bridges

EDP	LS _{OPL}	LS _{DPL}	LS _{UPL}	Collapse threshold
Longitudinal displacement ductility of pier walls, pir_L	1.0	2.3	3.3	4.5
Longitudinal deformation of abutments, abt_L (mm)	25	50.1	-64	n.a
Longitudinal deformation in bearings, brg_L (mm)	29	104	136	387
Transverse displacement ductility of pier walls, pir_T	1.0	2.1	3.4	6.7
Transverse deformation of abutments, abt_T (mm)	25	50.1	61	n.a
Transverse deformation in bearings, brg_T (mm)	29	91	142	n.a
Pier wall base shear in longitudinal direction, Vs_L (kN)	n.a	n.a	n.a	310

To allocate numerical LS values for the highway bridge components a prescriptive approach is adopted for this study, so that the numerical LSs in the OPL, DPL and UPL are prescribed based on the bridge dynamic behaviour (Nielson and DesRoches 2007). For this purpose, six EDPs

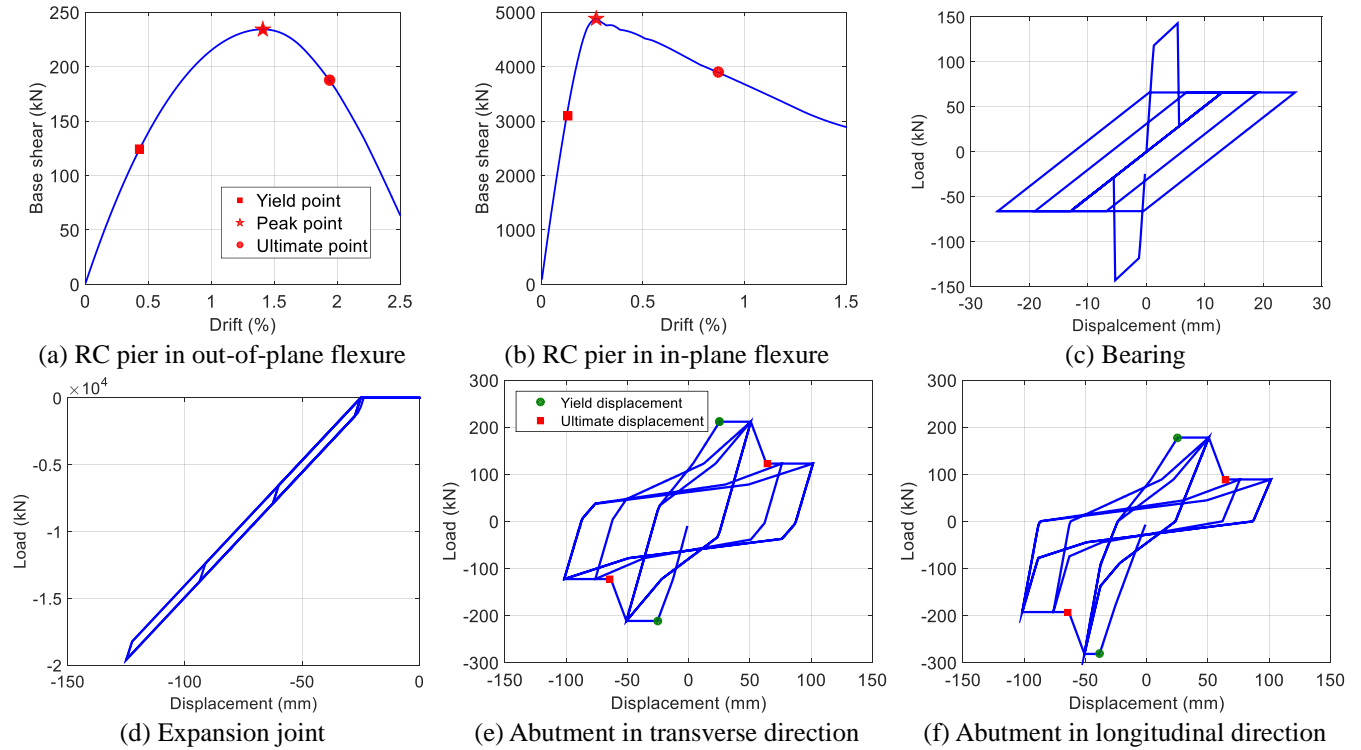


Fig. 8 Dynamic behaviour and seismic responses of bridge components

are nominated to be investigated by the seismic fragility function. These EDPs and the associated median LS values at the OPL, DPL and UPL (i.e., LS_{OPL} , LS_{DPL} and LS_{UPL}) are summarised in Table 4. It is to note that the displacement ductility is evaluated as the maximum transient drift in the RC piers normalised by the yield drift values (see Figs. 8(a) and 8(b)). In addition, four collapse thresholds are considered and presented in Table 4 (i.e., pir_L , brg_L , pir_T and Vs_L). Note that the Vs_L response is only considered for investigating the collapse stage. The base shear capacity is calculated according to the equation proposed by Setzler and Sezen (2008). The uncertainty of the nominated LS values is accounted for through a subjective manner (Benjamin and Cornell 1970), by assuming a lognormal distribution for these values and assigning a prescriptive coefficient of variation which equals 0.3, 0.45 and 0.6 for the bridge performance levels OPL, DPL and UPL, respectively. The performance of highway bridges in its entirety (i.e., at the system-level) is investigated through the application of “cut-set” definition (Franchin and Pinto 2009), Y_{LS} , which is defined as the maximum of the critical EDPs normalised by the corresponding LS values, as follow

$$Y_{LS} = \max_i^{N_{mech}} \max_j^{N_{ele}} \frac{EDP_{ji}}{LS_{ji}} \quad (3)$$

where N_{mech} is the number of potential failure mechanisms being considered, N_{ele} is the number of components taking part in the i^{th} failure mechanism and, EDP_{ji} and LS_{ji} are the seismic demand and limit-state, respectively, evaluated for the i^{th} mechanism of the j^{th} component.

5. Seismic fragility results

5.1 Validation of ECA method

To validate the ECA method, a seismic fragility assessment is also carried out by the rigorous IDA method for three sampled bridge models (i.e., No. 3, 14, 20, in Table 2), through performing THA at fifteen IMs (i.e., 0.1, 0.2, 0.3, 0.4, 0.5, 0.6, 0.7, 0.8, 0.9, 1.0, 1.1, 1.3, 1.5, 1.75, 2.0 g). Fig. 9 illustrates the seismic fragility results by the OCA, SCA, ECA and IDA methods for the highway bridge model No. 14 with GMR suite #3 (see Table 1). Detailed comparison of seismic fragility results by methods, for different combinations of the three bridge models and the four selected GMR suites, can be found in the work by Ghalami Sfahani (2017).

The values of the regression parameter “ b ” for different fragility assessment methods are compared in Fig. 9(a), which represent the slope of the median fit line, $\eta_{EDP/IM}$, in the sampling logarithmic space. As seen, the discrepancy between the OCA and IDA methods decreases as compared to that between OCA and SCA method. The ECA slightly improves the agreement with the IDA result. Nevertheless, the advantage of performing ECA is particularly evident considering the regression parameter $\beta_{EDP/IM}$ compared in Fig. 9(b): while the OCA and SCA methods evaluate a constant value, the ECA gives variable $\beta_{EDP/IM}$ values at the increasing IMs similar to the IDA method. This observation highlights the significance of using a scaled IM level beside the original one in the ECA method. As shown in this figure, the ECA method preserves a steady agreement with the IDA results over the entire IM range of interest. The non-collapse seismic fragility curves at the OPL, DPL and UPL are also generated by the OCA, SCA, ECA and IDA methods which are illustrated in Figs. 9(c)-(e). It is

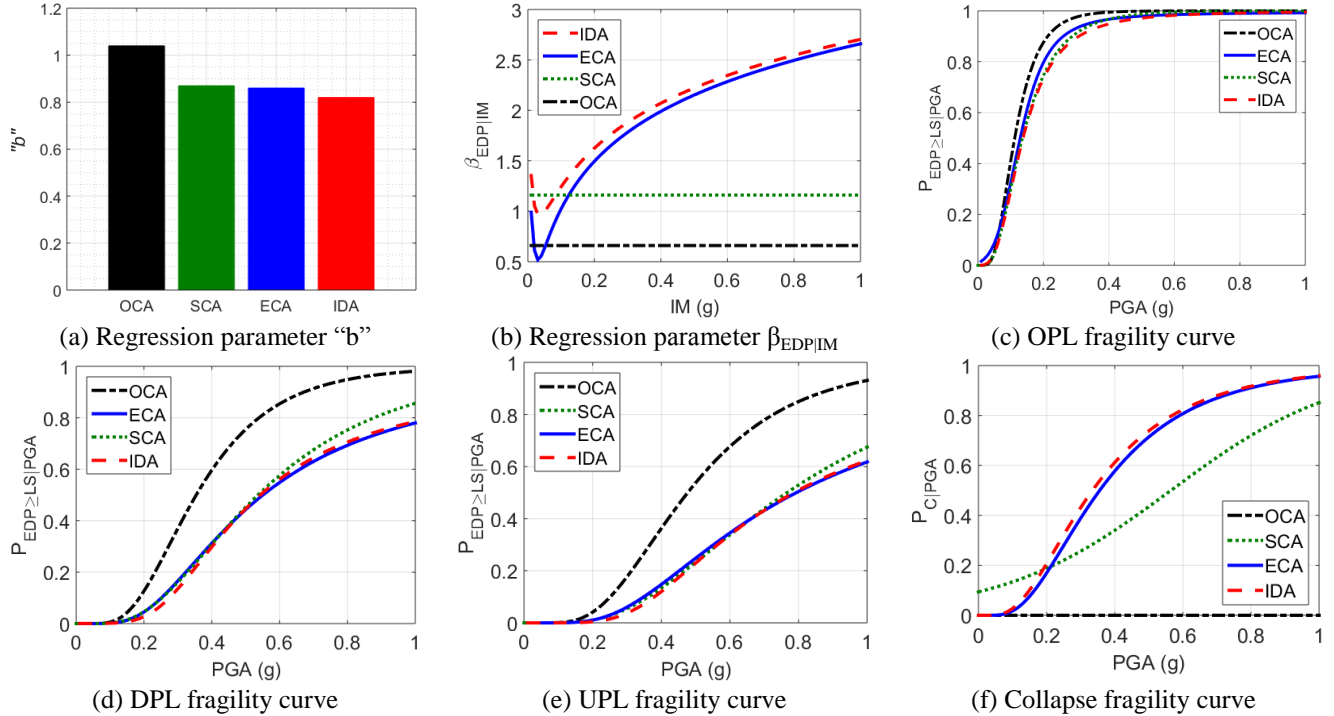


Fig. 9 Validation of seismic fragility results for sample highway bridge model #14

Table 5 Computational time using a 2.50-GHz Intel Core i5 2520M processor with 8 GB of 1333-MHz DDR3 RAM memory

Fragility assessment method	Number of performed THA	Computational time (hr)
OCA	300	45
SCA	300	43
ECA	600	87
IDA	4500	616

recognised that the OCA fragility curve can only be acceptable for the OPL as the inconsistency between OCA and IDA curves largely increases with the high nonlinearity at DPL and UPL. Finally, the collapse seismic fragility curves due to the four methods are compared in Fig. 9(f). As seen, the OCA method fails to identify any IM_C by the utilised GMRs and, thus, it estimates $P_{C|IM}=0$ over the entire range of IMs. This issue is recovered by the SCA method, to some extent. However, once the ECA method is utilised a remarkable agreement with the IDA collapse fragility curve can be achieved. Consequently, it is concluded that the ECA is a reliable and versatile method for seismic fragility assessment.

Further, the cost-efficiency of the OCA, SCA, ECA and IDA methods can be compared through Table 5, where the total computational time for performing seismic fragility assessment over the three adopted bridge models subjected to the four selected GMR suites in OpenSees is numerically summarised. Note that, although OCA and SCA are more effective in computation, as shown in Table 5, their performances in seismic fragility assessment have demonstrated to be less satisfactory than the ECA method. Given that ECA combines the OCA and SCA data in its operation, the computational time for performing ECA is

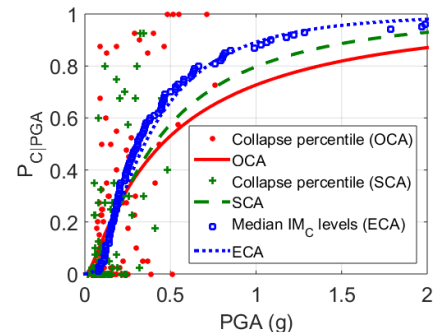


Fig. 10 Representative collapse seismic fragility curves for the southeast Queensland highway bridges

the sum of that required by the OCA and SCA. Nevertheless, compared to the conventional IDA which requires more than 25 days, the use of the proposed ECA method for seismic fragility assessment saves a remarkable computational time.

5.2 Representative bridge fragility curves

The seismic fragility assessment of the existing highway bridges in southeast Queensland is performed by the ECA method, using the forty sampled bridge models and one-hundred selected GMRs. For this purpose, 4000 THA are initially performed based on the OCA method and, then, another 4000 THA are carried out based on the SCA method using the “transition” scaling approach. Fig. 10 demonstrates the generated collapse seismic fragility curves for these bridges. In this figure, the red datapoints and the green cross marks represent the percentiles of collapse at the IM levels of utilised GMRs by the OCA and SCA methods, respectively. This percentile is simply calculated

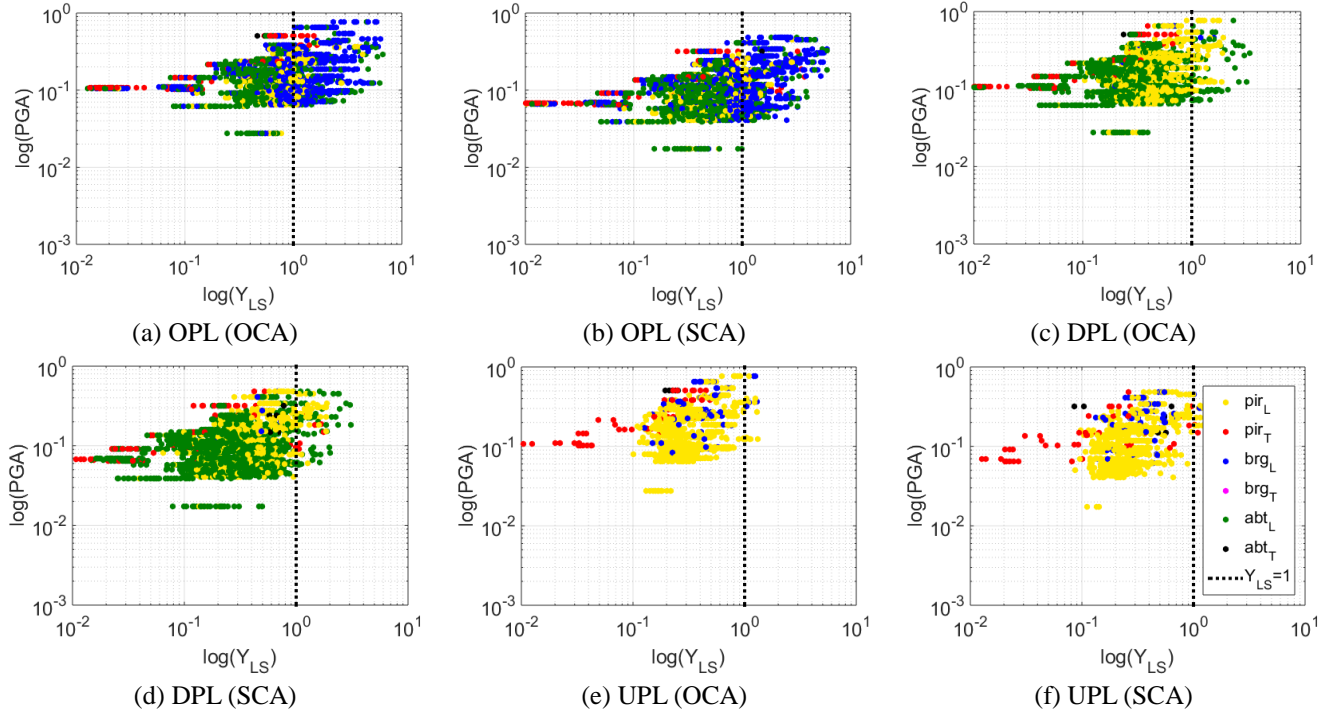


Fig. 11 Distributions of non-collapse cut-sets at different bridge performance levels

as the fraction of collapse cases counted in the sample of forty bridge models, by each GMR. For the ECA method, instead of such percentiles, forty IM_C levels are evaluated by each GMR (i.e., one for each sample bridge model) and the median of these IM_C values is then sampled to generate an empirical CDF of IM_C levels (blue squares in Fig. 10). The representative collapse seismic fragility curves are generated using the maximum likelihood method curve fitting method (Baker 2015). It seems that the OCA and SCA methods underestimate the collapse probability compared to the ECA method as IM increases. To investigate the non-collapse seismic fragility of the southeast Queensland highway bridges, the quantified system-level cut-sets, Y_{LS} , at different bridge performance levels, are scattered in Fig. 11. The datapoints illustrated by various colours in this figure indicate different EDPs (see Table 4) utilised for seismic fragility assessment. As such, the multiplicity of a specific colour implies that the corresponding EDP is the dominant seismic response. To generate the non-collapse fragility curves, based on the ECA method, the Y_{LS} sampled by the OCA (Figs. 11(a), 11(c) and 11(e)) are paired with the corresponding Y_{LS} sampled by the SCA (Figs. 11(b), 11(d) and 11(f)) to evaluate the IM_{LS} . Note that this is the IM level at which the median fit and the $Y_{LS}=1$ lines intersect in the sampling logarithmic space. The non-collapse fragility curves can then be generated identically to the collapse fragility curves where only the IM_C is substituted by the IM_{LS} .

Fig. 12(a) illustrates the non-collapse seismic fragility curves of bridge components generated for the nominated EDPs, by the ECA method. It appears that the highway bridges are more fragile with respect to their longitudinal seismic responses compared to their transverse directions. In particular, this is apparent considering the seismic

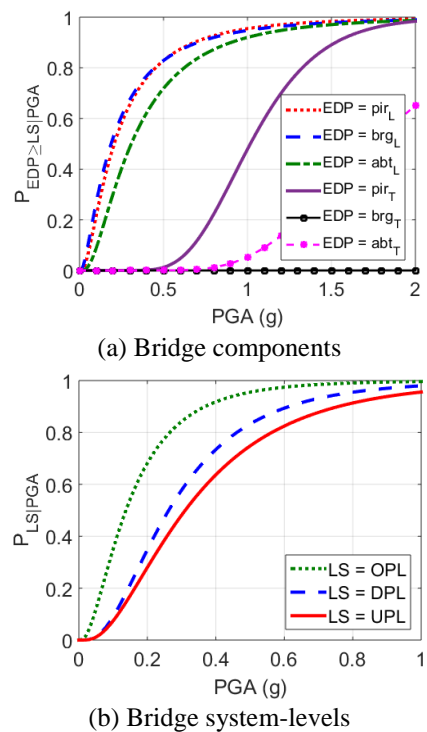


Fig. 12 Representative non-collapse seismic fragility curves for the southeast Queensland highway bridges

responses of the bearings (i.e., brg_L and brg_T) in which failure due to excessive brg_T responses seems to be improbable.

It is also recognised that the pier wall is the most vulnerable bridge component considering both longitudinal and transverse directions. The total probability of meeting or exceeding different bridge performance levels, $P_{LS/IM}$, is

demonstrated through the system-level fragility curves shown in Fig. 12(b). These curves are generated as the representative non-collapse seismic fragility curves for existing highway bridges in southeast Queensland. According to these curves, the median seismic fragility (i.e., 50% probability of exceedance) of highway bridges in southeast Queensland is estimated to be PGA=0.14 g, 0.26 g and 0.32 g in the OPL, DPL and UPL, respectively.

6. Conclusions

Reliable risk estimation of civil infrastructure is a key element to ensure the operational performance of public assets and improve their resilience against future disasters. In this study, an existing OCA methodology was improved by the proposed ECA method to generate representative and reliable seismic fragility curves for highway bridges ubiquitous in southeast Queensland. It is shown that performing the ECA method ensures the attainment of stable collapse fragility curves, in a close agreement with the rigorous IDA method. Employing the ECA method requires two THA with each selected GMR, at the original and scaled IM levels, which reduces a considerable amount of computational time in comparison to the IDA method performed at ten or more IMs. There is also a remarkable agreement between the non-collapse fragility curves generated by the ECA and the IDA methods. The fragility assessment by the ECA method shows that the median seismic fragility of existing bridges in southeast Queensland is PGA=0.14 g in the OPL. This means that 50% of existing bridges in this region will damage if an earthquake with such an intensity occurs. The median seismic fragility at the DPL, UPL and collapse stage are estimated to be PGA=0.26 g, 0.32 g and 0.35 g, respectively. Also, the RC pier walls are found to be the most vulnerable bridge components. The outcome of this study can be utilised as a useful tool for the local bridge agencies and transportation authorities in their maintenance, rehabilitation, and repair (MR&R) activities, in conjunction with relevant decision-making tools for long-term bridge management.

References

- Akhoondzade-Noghabi, V. and Bargi, K. (2016), "Decision-making of alternative pylon shapes of a benchmark cable-stayed bridge using seismic risk assessment", *Earthq. Struct.*, **11**(4), 583-607.
- Ancheta, T.D., Darragh, R.B., Stewart, J.P., Seyhan, E., Silva, W.J., Chiou, B.S.J., Wooddell, K.E., Graves, R.W., Kottke, A.R. and Boore, D.M. (2014), "NGA-West2 database", *Earthq. Spectra*, **30**(3), 989-1005.
- AS1170.4 (2007), Structural Design Actions Part 4: Earthquake Actions in Australia, A. Standard, NSW, Sydney.
- AS5100.2 (2004), Bridge Design Part 2: Design Loads, AS5100.2. A. Standard, NSW, Sydney.
- Aviram, A., Mackie, K.R. and Stojadinovic, B. (2008), "Effect of abutment modeling on the seismic response of bridge structures", *Earthq. Eng. Eng. Vib.*, **7**(4), 395-402.
- Ayyub, B.M. and Lai, K.L. (1989), "Structural reliability assessment using latin hypercube sampling", *Proceedings of ICOSSAR'89, The 5th International Conference on Structural Safety and Reliability*, San Francisco, CA, USA, ASCE.
- Baker, J.W. (2010), "Conditional mean spectrum: Tool for ground-motion selection", *J. Struct. Eng.*, **137**(3), 322-331.
- Baker, J.W. (2015), "Efficient analytical fragility function fitting using dynamic structural analysis", *Earthq. Spectra*, **31**(1), 579-599.
- Benjamin, J.R. and Cornell, C.A. (1970), *Reliability, Statistics and Decision for Civil Engineers*, McGraw Hill, New York, NY.
- Caltrans, C. (2013), Seismic Design Criteria (SDC), v 1.7, California Department of Transportation, Sacramento, CA.
- Cardone, D., Perrone, G. and Sofia, S. (2011), "A performance-based adaptive methodology for the seismic evaluation of multi-span simply supported deck bridges", *Bull. Earthq. Eng.*, **9**(5), 1463.
- Choi, E., DesRoches, R. and Nielson, B. (2004), "Seismic fragility of typical bridges in moderate seismic zones", *Eng. Struct.*, **26**(2), 187-199.
- Cornell, C. (1968), "Engineering seismic risk analysis", *Bull. Seismol. Soc. Am.*, **58**(5), 1583-1606.
- Cornell, C., Jalayer, F., Hamburger, R. and Foutch, D.A. (2002), "Probabilistic basis for 2000 SAC federal emergency management agency steel moment frame guidelines", *J. Struct. Eng.*, **128**(4), 526-533.
- Cornell, C. and Krawinkler, H. (2000), "Progress and challenges in seismic performance assessment", *PEER Center New.*, **3**, 1-3.
- DesRoches, R., Leon, R.T. and Dyke, S. (2003), "Response modification of bridges", Mid-America Earthquake Center CD Release, 03-08.
- Ebrahimian, H., Jalayer, F., Asprone, D., Lombardi, A.M., Marzocchi, W., Prota, A. and Manfredi, G. (2014), "A performance-based framework for adaptive seismic aftershock risk assessment", *Earthq. Eng. Struct. Dyn.*, **43**(14), 2179-2197.
- Ebrahimian, H., Jalayer, F. and Manfredi, G. (2015), "Seismic retrofit decision-making of bridges based on life-cycle cost criteria", *Proceedings of the 5th ECCOMAS Thematic Conference on Computational Methods in Structural Dynamics and Earthquake Engineering*, Crete Island, Greece.
- Fajfar, P. (2000), "A nonlinear analysis method for performance-based seismic design", *Earthq. Spectra*, **16**(3), 573-592.
- Franchin, P. and Pinto, P.E. (2009), "Allowing traffic over mainshock-damaged bridges", *J. Earthq. Eng.*, **13**(5), 585-599.
- Ghalami Sfahani, M. (2017), "Seismic fragility assessment of highway overpasses with pier walls in low-to-moderate seismic zones", Ph.D. Dissertation, Griffith University.
- Ghalami Sfahani, M., Guan, H. and Loo, Y.C. (2015), "Seismic reliability and risk assessment of structures based on fragility analysis-A review", *Adv. Struct. Eng.*, **18**(10), 1653-1669.
- Ghalami Sfahani, M., Guan, H., Lu, X. and Loo, Y.C. (2015), "Probabilistic evaluation of the seismic performance of a concrete highway bridge in Queensland", *Proceedings of the Second International Conference on Performance-based and Lifecycle Structural Engineering (PLSE 2015)*, Brisbane, Australia.
- Günay, S. and Mosalam, K.M. (2013), "PEER performance-based earthquake engineering methodology, revisited", *J. Earthq. Eng.*, **17**(6), 829-858.
- Jalayer, F. (2003), "Direct probabilistic seismic analysis: implementing non-linear dynamic assessments", Ph.D. Dissertation, Stanford University.
- Jayaram, N., Lin, T. and Baker, J.W. (2011), "A computationally efficient ground-motion selection algorithm for matching a target response spectrum mean and variance", *Earthq. Spectra*, **27**(3), 797-815.
- Kaviani, P., Zareian, F. and Taciroglu, E. (2012), "Seismic behavior of reinforced concrete bridges with skew-angled seat-type abutments", *Eng. Struct.*, **45**, 137-150.

- Leonard, M., Burbidge, D., Allen, T., Robinson, D., McPherson, A., Clark, D. and Collins, C. (2014), "The challenges of probabilistic seismic-hazard assessment in stable continental interiors: An Australian example", *Bull. Seismol. Soc. Am.*, **104**(6), 3008-3028.
- Leonard, M., Burbidge, D. and Edwards, M. (2013), "Atlas of seismic hazard maps of Australia-Seismic hazard maps, hazard curves and hazard spectra", *Geoscience Australia Record*.
- Lu, X., Xie, L., Guan, H., Huang, Y. and Lu, X. (2015), "A shear wall element for nonlinear seismic analysis of super-tall buildings using OpenSees", *Finite Elem. Anal. Des.*, **98**, 14-25.
- McKenna, F., Fenves, G., Jeremic, B. and Scott, M. (2015), "Open system for earthquake engineering simulation, 2000", <http://opensees.berkeley.edu>.
- Muthukumar, S. and DesRoches, R. (2006), "A Hertz contact model with non-linear damping for pounding simulation", *Earthq. Eng. Struct. Dyn.*, **35**(7), 811-828.
- Nielson, B.G. and DesRoches, R. (2007), "Seismic fragility methodology for highway bridges using a component level approach", *Earthq. Eng. Struct. Dyn.*, **36**(6), 823-839.
- Olmos, B.A., Jara, J.M. and Jara, M. (2012), "Influence of some relevant parameters in the seismic vulnerability of RC bridges", *Earthq. Struct.*, **3**(3-4), 365-381.
- Padgett, J.E. and DesRoches, R. (2008), "Methodology for the development of analytical fragility curves for retrofitted bridges", *Earthq. Eng. Struct. Dyn.*, **37**(8), 1157-1174.
- Scott, M.H. and Fenves, G.L. (2006), "Plastic hinge integration methods for force-based beam-column elements", *J. Struct. Eng.*, **132**(2), 244-252.
- Setzler, E.J. and Sezen, H. (2008), "Model for the lateral behavior of reinforced concrete columns including shear deformations", *Earthq. Spectra*, **24**(2), 493-511.
- Somerville, P., Graves, R., Collins, N., Song, S.G., Ni, S. and Cummins, P. (2009), "Source and ground motion models for Australian earthquakes", *Proceedings of 2009 Annual Conference of Australian Earthquake Engineering Society*.
- Vamvatsikos, D. and Cornell, C.A. (2002), "Incremental dynamic analysis", *Earthq. Eng. Struct. Dyn.*, **31**(3), 491-514.

KT